The Astrophysical Journal, 836:247 (8pp), 2017 February 20 https://doi.org/10.3847/1538-4357/836/2/247

Electron Heating at Kinetic Scales in Magnetosheath Turbulence

Alexandros Chasapis[1], W. H. Matthaeus[1], T. N. Parashar[1], O. LeContel[2], A. Retinò[2], H. Breuillard[2], Y. Khotyaintsev[3], A. Vaivads[3], B. Lavraud[4,5], E. Eriksson[3], T. E. Moore[6], J. L. Burch[7], R. B. Torbert[8], P.-A. Lindqvist[9], R. E. Ergun[10], G. Marklund[9], K. A. Goodrich[10], F. D. Wilder[10], M. Chutter[8], J. Needell[8], D. Rau[8], I. Dors[8], C. T. Russell[11], G. Le[6], W. Magnes[12], R. J. Strangeway[11], K. R. Bromund[6], H. K. Leinweber[11], F. Plaschke[12], D. Fischer[12], B. J. Anderson[13], C. J. Pollock[6], B. L. Giles[6], W. R. Paterson[6], J. Dorelli[6], D. J. Gershman[6], L. Avanov[6], and Y. Saito[14]

[1] University of Delaware, Newark, Delaware, USA; chasapis@udel.edu
[2] Laboratory de Physique des Plasmas, Paris, France
[3] Swedish Institute of Space Physics, Uppsala, Sweden
[4] Institut de Recherche en Astrophysique et Plantologie, Université de Toulouse (UPS), France
[5] Centre National de la Recherche Scientifique, UMR 5277, Toulouse, France
[6] NASA Goddard Space Flight Center, Greenbelt, MD, USA
[7] Southwest Research Institute, San Antonio, TX, USA
[8] University of New Hampshire, Durham, NH, USA
[9] Royal Institute of Technology, Stockholm, Sweden
[10] University of Colorado, Laboratory for Atmospheric and Space Physics, Boulder, CO, USA
[11] University of California, Los Angeles, CA, USA
[12] Space Research Institute, Austrian Academy of Sciences, Graz, Austria
[13] Johns Hopkins University Applied Physics Laboratory, Laurel, MD, USA
[14] Institute for Space and Astronautical Science, Sagamihara, Japan

Received 2016 September 13; revised 2016 December 23; accepted 2016 December 28; published 2017 February 24

Abstract

We present a statistical study of coherent structures at kinetic scales, using data from the *Magnetospheric Multiscale* mission in the Earth's magnetosheath. We implemented the multi-spacecraft partial variance of increments (PVI) technique to detect these structures, which are associated with intermittency at kinetic scales. We examine the properties of the electron heating occurring within such structures. We find that, statistically, structures with a high PVI index are regions of significant electron heating. We also focus on one such structure, a current sheet, which shows some signatures consistent with magnetic reconnection. Strong parallel electron heating coincides with whistler emissions at the edges of the current sheet.

Key words: acceleration of particles – magnetic reconnection – plasmas – turbulence

1. Introduction

Turbulent plasmas are characterized by the formation of intermittent structures. Energy is injected by large-scale processes and cascades down to kinetic scales, where it is dissipated. Identifying the mechanism of energy dissipation at kinetic scales in turbulent plasmas is a long standing research topic, one that has been challenging to address because of the scarcity of high-resolution multi-point in situ measurements. The *Magnetospheric Multiscale* (*MMS*) mission (Burch et al. 2016) is equipped with instrumentation that provides us with high time resolution multi-spacecraft field and particle data, enabling us to start addressing some critical questions related to turbulent dissipation at kinetic scales. Numerous mechanisms have been invoked to study the transfer of turbulent energy into thermal degrees of freedom in weakly collisional plasmas, such as the solar wind and the Earth's magnetosheath. Examples include wave-particle interactions such as cyclotron resonance (Hollweg & Isenberg 2002) and Landau-damping (Howes 2015), stochastic heating (Bourouaine & Chandran 2013; Xia et al. 2013), and interactions with intermittent structures (Sundkvist et al. 2007; Osman et al. 2011; Parashar et al. 2011; Wan et al. 2016). The present study focuses on intermittent structures, where various mechanisms can lead to heating and acceleration.

Theoretical (e.g., Shay et al. 2014; Haggerty et al. 2015) as well as observational studies (e.g., Sundkvist et al. 2007; Osman et al. 2011; Servidio et al. 2011; Chasapis et al. 2015) suggest that magnetic reconnection, that has been observed in the laboratory as well as in space plasmas (Ren et al. 2005; Gosling 2007; Retinò et al. 2007; Shibata et al. 2007; Stevens 2009; Cirtain et al. 2013; Osman et al. 2014), and related activity associated with concentration of electric current are significant contributors to dissipation of magnetic field energy and conversion into particle heating and acceleration. Here we use data from the *MMS* spacecraft (Burch et al. 2016), focusing on an interval where the spacecraft are in Earth's magnetosheath. A high level of electromagnetic fluctuations is observed in this region, offering a useful environment for in situ study of turbulent dissipation at kinetic scales. Additionally, the high time resolution data provided by *MMS*, combined with the small separation between the spacecraft, allows us to examine some of these issues. Specifically, we are able to reliably measure the electron temperature within ion-scale structures and to follow its evolution within such structures. These measurements allow us to study the properties of electron heating within ion-scale intermittent structures and to compute robust statistics of the electron heating occurring in kinetic scale structures.

2. Data

The *MMS* spacecraft were launched in 2015 March in orbit around Earth. During late 2015 until early 2016, the apogee was at $12R_E$ on Earth's day side. This orbit allowed the spacecraft to cross the Earth's magnetopause and venture into the Earth's magnetosheath for extended periods. Here we focus on one such traversal from 2016 January 11. From 00:25 UT until 01:15 UT the spacecraft encountered strong magnetic field turbulence ($\Delta B/B \sim 1$) typically associated with the magnetosheath downstream of the quasi-parallel shock. During this period, around 0100 UT, an interval of three minutes of Burst Mode was selected by the Scientist-In-The-Loop (Baker et al. 2016).

The burst mode magnetic and electric field data were provided by the FIELDS instrument suite (Torbert et al. 2016). Specifically, the flux-gate magnetometer measured the DC magnetic field at a resolution of 128 Hz (Russell et al. 2016), and the search-coil magnetometer up to 8 kHz (Le Contel et al. 2016). The electric field is measured by two instruments with a resolution of 8 kHz. The axial double probe (Ergun et al. 2016), which measures the electric field along the spin axis of the spacecraft, and the spin-plane double probe, which takes measurements along the spin plane of the spacecraft (Lindqvist et al. 2016).

The FPI instrument (Pollock et al. 2016) measures the electron distribution functions and calculates the moments of those distributions with a cadence of 30 ms. We use the measurements provided by the EDP (Lindqvist et al. 2016) instrument to correct for the photo-electrons and the effects of the spacecraft potential on the electron distribution functions.

The interval of interest can be seen in Figure 1. Panel B of Figure 1 shows survey magnetic field data by MMS3 as the spacecraft travel in the magnetosheath. Strong turbulence is observed in an interval of about one hour between 00:25 UT and 01:15 UT. Panel C shows MMS3 magnetic field measurements from a burst data interval, which is used for the statistical study presented here. Panel D shows one particular structure that is examined in detail in Section 5.

3. Detection of Intermittent Structures

The first step is to detect the intermittent magnetic structures that exist in the burst interval. In order to detect intermittent structures, we use the partial variance of increments (PVI) method (Greco et al. 2008, 2009). This method relies on the calculation of magnetic field increments normalized by the variance of the magnetic field.

Most previous studies have used this method for spatial increments in simulation and as temporal increments for single-spacecraft data. Here we adopt the approach used in Chasapis et al. (2015), which computes spatial increments between the 4 *MMS* spacecraft, therefore taking advantage of the multi-spacecraft measurements instead of employing the Taylor frozen-in flow hypothesis. For this interval, the separation between the spacecraft is 30–40 km and the ion gyro-radius is $\sim$80 km. Therefore, a multi-spacecraft approach is well-suited to focus on ion and sub-ion scales. In order to calculate the PVI index, following the method presented in Greco et al. (2008) as adapted in Chasapis et al. (2015) for multi-spacecraft data, we compute increments of the magnetic field as follows

$$|\Delta \boldsymbol{B}_{ij}(t)| = |\boldsymbol{B}_i(t) - \boldsymbol{B}_j(t)| \tag{1}$$

where t is the time of every measurement and where $i, j = 1, 2, 3, 4$ correspond to the four *MMS* spacecraft. From that, we calculate the normalized PVI index (PVI index)

$$\mathrm{PVI}_{ij}(t) = \sqrt{\frac{|\Delta \boldsymbol{B}_{ij}(t)|^2}{\langle |\Delta \boldsymbol{B}_{ij}|^2 \rangle}} \tag{2}$$

where $\langle |\Delta \boldsymbol{B}_{ij}|^2 \rangle$ denotes the time average over the span of the time-series. In the case of this study, the average was calculated over the three-minute burst data interval.

Intermittent structures that form in turbulence are usually associated with a sharp variation of the magnetic field. Therefore, we expect to observe a peak of the PVI index as the spacecraft cross through such structures. Because events with a high PVI index are associated with magnetic discontinuities, based on Ampere's law, it is expected that a current would be associated with such structures (Greco et al. 2008; Chasapis 2015). The statistical association of PVI events and current is shown in Figure 2. However, whether these events can be identified as rotational discontinuities, tangential discontinuities, or localized currents associated with other kinds of intermittent structures cannot be explicitly determined by this method. A more detailed analysis is required (for example, see Greco et al. 2009; Li 2008; Zhdankin et al. 2013; Neugebauer 2006; Rappazzo & Parker 2013; and references therein) to classify the coherent structures that PVI can detect.

It is worth emphasizing that intermittent structures in plasma turbulence might correspond to localized structures in any of several different dynamical variables. Often such structures are in close proximity to strong currents (Servidio et al. 2012; Parashar & Matthaeus 2016). Such structures might also be compressive in nature (Perrone et al. 2016). It is our intention to look at the statistical behavior of heating within intermittent structures, regardless of how they might be classified (shocks, directional discontinuities, etc.). The classification of intermittent structures in space plasma turbulence is beyond the scope of this paper.

For the three-minute interval of burst data, we detected in total 312 PVI events with PVI $>$ 1. Of those, 24 had PVI $>$ 3. The relative population of high and low PVI events (7.7%) is consistent with previous statistical studies that used this methodology in numerical simulations (Servidio et al. 2011) and observations in the solar wind (Osman et al. 2014) and the Earth's magnetosheath (Chasapis et al. 2015).

4. Statistics of Intermittency and Heating

Next, we look into the evolution of the electron temperature within the whole population of PVI events, in order to examine the presence of significant electron heating and its dependence on the value of the PVI index of each structure.

The high time resolution (30 ms) electron moments and distributions provided by the FPI instrument suite of the *MMS* mission allow us to robustly and consistently study the evolution of the electron temperature at such small scales.

For each PVI event, we calculated the temperature increase ΔT_e as an estimation of the electron heating within. This was estimated for each spacecraft by computing the maximum minus the average temperature $\Delta T_e = T_{e\mathrm{MAX}} - \langle T_e \rangle$ over the duration of each PVI event. The four such values obtained by each spacecraft were then averaged in order to yield an estimate of the electron heating for each PVI event. The same approach was followed in Chasapis et al. (2015). The validation and robustness of such an approach was examined in more detail in Chasapis (2015).

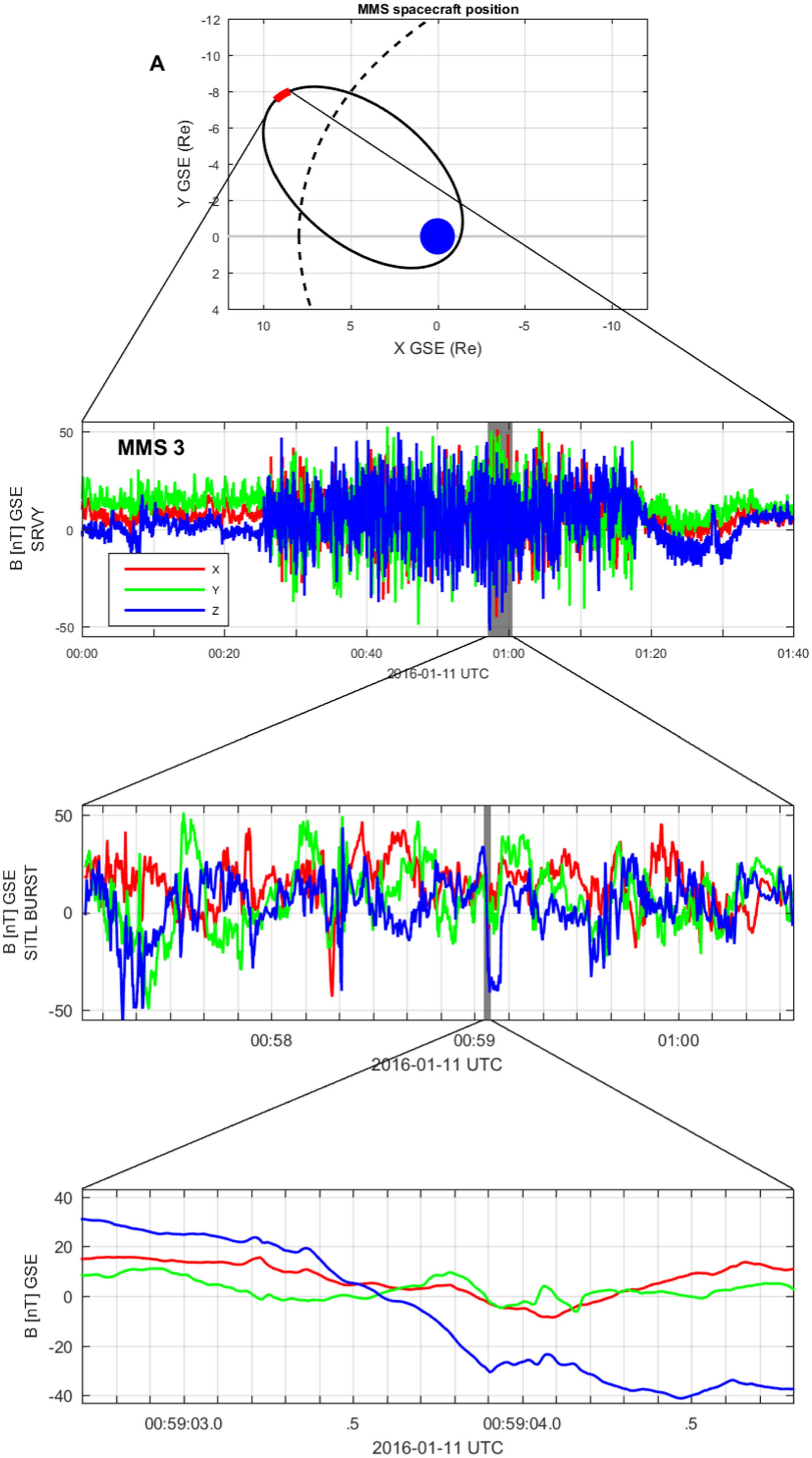

Figure 1. *MMS* spacecraft position and magnetic field measurements by MMS3 in the Earth's magnetosheath. Panel A shows the spacecraft orbit (black line). The interval of interest is highlighted in red. The dashed line indicates the position of the magnetopause. Panel B fast survey magnetic field data in the magnetosheath turbulence. Panel C shows the burst data interval. Panel C shows one current sheet detected within that interval.

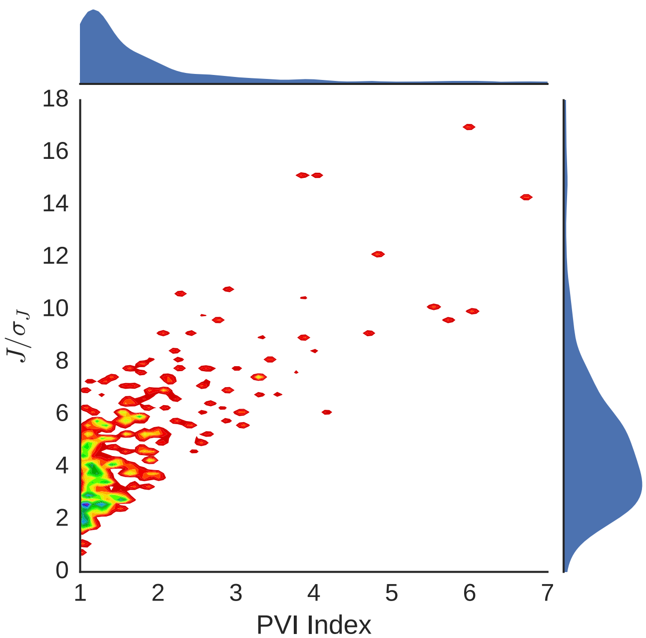

Figure 2. Kernel density estimate of the maximum of the joint distribution of the magnitude of the current $|\boldsymbol{J}|$ measured by the FPI instrument and the PVI index for the detected PVI events. The reduced distributions of the magnitude of the current $|\boldsymbol{J}|$ and the PVI index are shown separately in blue on the right and the upper margins of the plot respectively. The Pearson correlation coefficient for the data is 0.85.

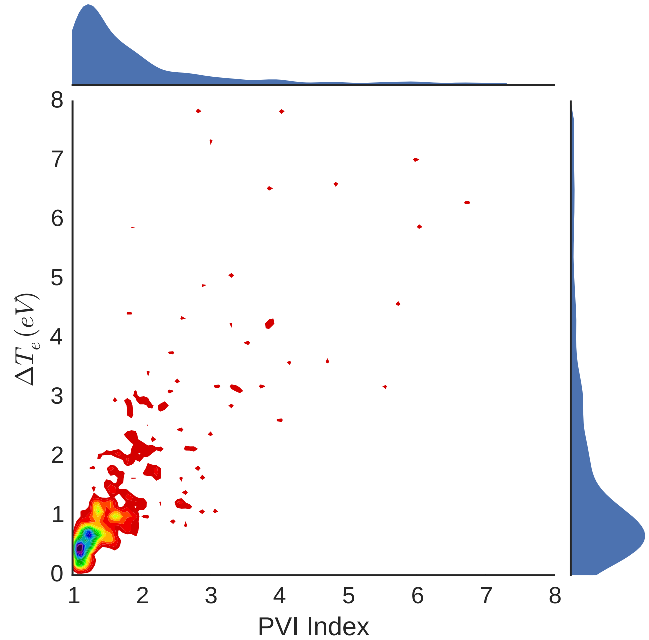

Figure 3. Kernel density estimate of the joint distribution of the electron heating ΔT_e and the PVI index for the detected intermittent structures. The data show a high degree of correlation even for low PVI values. The reduced distributions of the electron heating and the PVI index are shown separately in blue on the right and the upper margins of the plot respectively. The Pearson correlation coefficient for the data is 0.8.

Figure 3 shows the results of this statistical analysis. The overwhelming majority of low PVI (PVI $<$ 3) events do not show significant electron heating. Strong electron heating is observed within the high PVI (PVI $>$ 3) events. The Pearson correlation coefficient for the ΔT_e and the PVI index is $\sim$0.8. This indicates that, even for low PVI events, where the heating is low, a larger value of PVI corresponds to more significant electron heating. This can be seen as a linear trend in the data even for small PVI values. The effect is more pronounced for the cases with PVI $>$ 3. The clear positive correlation between observed heating and the PVI index supports the hypothesis that coherent structures are sites of dissipation and electron heating. This is consistent with previous observational and numerical studies (Servidio et al. 2011; Osman et al. 2014; Chasapis et al. 2015)

Finally, the observed heating appears to be predominantly in the direction parallel to the magnetic field. Specifically, for 65% of the total PVI events, the increase in the parallel temperature is higher than the perpendicular one. This percentage goes up to 80% for the cases with PVI $>$ 3.

Past studies have proposed that magnetic reconnection has a high probability to take place within high PVI events (Servidio et al. 2011; Osman et al. 2014). This could explain the electron heating observed in those structures. However, further study is needed in order to identify the nature of those structures and to determine whether magnetic reconnection is indeed the mechanism behind the observed heating, and whether there are other mechanisms at play.

5. Electron Heating in a Thin Current Sheet

We chose one particular PVI event, specifically a thin current sheet shown in Figure 1, in order to examine in more detail the mechanisms that lead to electron heating. The region near this current sheet can be seen in more detail in Figure 4. It has a strong shear ($\sim$160°) and appears to be symmetric in magnetic field and density (not shown). Using the minimum variance analysis, we were able to determine the orientation of the current sheet. This allowed us to define a right-handed reference frame of the current sheet (l, m, n), where (l) corresponds to the maximum variance component, (m) to the out-of-plane component and (n) to the component normal to the current sheet plane. Specifically, the maximum variance component was $l = (+0.306, +0.083, +0.949)$, the out-of-plane direction was $m = (-0.203, -0.968, +0.150)$, and the normal direction was $n = (+0.930, -0.238, -0.279)$. The ratio of the eigenvalues corresponding to the intermediate and minimum variance was 21, while the ratio of the maximum and intermediate eigenvalue was 16.

Using the timing of the crossing between the spacecraft (Paschmann & Daly 1998), we estimate independently the normal direction of the plane of the current sheet, as well as its velocity at $\sim$210 km s^{-1}. The normal direction given by the timing analysis agreed with the one obtained by the minimum variance analysis within a few degrees. Thus we were able to compute the electric field in the reference frame of the current sheet $\boldsymbol{E}' = \boldsymbol{E} - \boldsymbol{V}_{\rm CS} \times \boldsymbol{B}$. Given the approximate velocity of the current sheet and time it takes for the spacecraft to cross it, the thickness of the current sheet can be estimated at $\sim 2 - 4\rho_i$, where ρ_i is the ion gyro-radius, which for this interval has a value of $\rho_i \sim 80$ km.

Panel A of Figure 4 shows the magnetic field in the (l, m, n) frame of the current sheet. We observe the reversal of the maximum variance component across the current sheet. The out-of-plane component shows a bipolar signature consistent with the expected quadrupolar Hall magnetic field structure in a diffusion region when crossing perpendicular to the current sheet plane. The magnetic field in the direction normal to the plane of the current sheet has a small positive value. The

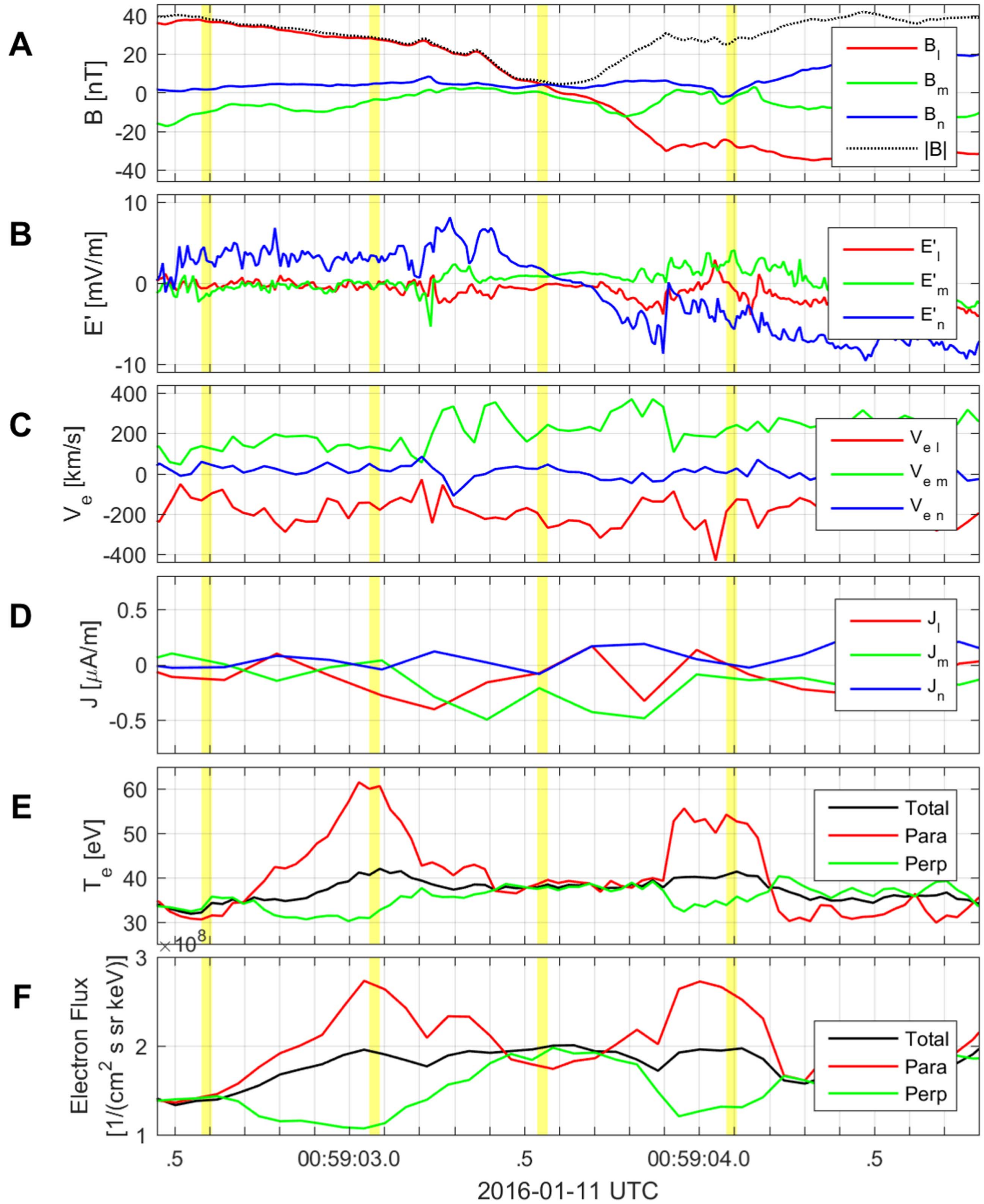

Figure 4. Thin current sheet in the Earth's magnetosheath observed by MMS3. The measurements are made over time in UTC, and are in the reference frame of the current sheet (l, m, n). The three directions (l, m, n) refer to the maximum variance component (l), the out-of-plane component (m), and the component normal to the current sheet plane (n). Panel A shows the magnetic field $\boldsymbol{B}$ as the spacecraft crosses the current sheet measured by FGM. Panel B shows the Electric field $\boldsymbol{E}'$ in the reference frame of the current sheet. Panel C shows the electron velocity in the current sheet frame measured by FPI. Panel D shows the current derived from the FPI ion and electron measurements. Panel E shows the total electron temperature as well as the electron temperature in the directions parallel and perpendicular to the magnetic field. Panel F shows the total electron flux for different pitch angles with respect to the magnetic field. The four regions highlighted in yellow mark, respectively, the inflow region, the right edge, the center and the left edge of the current sheet, which are examined in more detail in Figure 5.

bipolar Hall electric field can be seen in the normal component of the electric field, shown in Panel B of the same figure. These observations suggest that *MMS* spacecraft crossed near the diffusion region of this current sheet.

Specifically, the spacecraft appear to cross perpendicular to the plane of the current sheet in the $+n$ direction and in the $-l$ side if we consider the x-point at the zero of the (l, m, n) axes.

Panels C and D show, respectively, the electron velocity in the frame of the current sheet, and the current measured by the FPI instrument. We observe a negative out-of-plane current, consistent with the orientation of the current sheet with respect to the spacecraft. Additionally, the current sheet appears to be embedded in a fast flow of $\sim$200 km s^{-1} in the $-l$ and $+m$ direction. Finally, we calculated the quantity $\boldsymbol{E}' \cdot \boldsymbol{J}$ (not shown), which was on average positive during the crossing, indicating energy transfer from the magnetic field to the particles, consistent with the electron heating shown in Panel E.

As can be seen in Panel E of Figure 4, the observed electron heating appears to be localized in two distinct peaks lying on the edges of the current sheet. At these two regions a significant temperature increase $\sim$20 eV is observed in the direction parallel to the magnetic field, whereas in the perpendicular direction there is no variation with respect to the region outside the current sheet. In the center of the current sheet, the electron population is isotropic, with a temperature elevated by $\sim$5 eV with respect to the region outside of the current sheet, in both parallel and perpendicular directions. The electron flux, shown in Panel F of Figure 4, is higher in the directions parallel and anti-parallel to the magnetic field in the regions where the heating is observed, pointing to the presence of counter-streaming field-aligned electrons. These observations suggest that the *MMS* spacecraft likely crossed near the diffusion region of a thin reconnecting current sheet similar to the one first reported in Retinò et al. (2007).

In such a reconnecting current sheet, apart from Hall signatures and a specific pattern of electron heating, the observation of an electron jet is also expected. The absence of a conspicuous jet in Figure 4 Panel C (expected in the $-l$ direction), could be attributed to intermittent reconnection (Hasegawa et al. 2010) or the complex three-dimensional configuration within this region (Dmitruk & Matthaeus 2006), both of which are expected in such a turbulent environment. Finally, the example shown here is embedded in a large-scale fast flow in the $+y$ and $-z$ direction in GSE coordinates. Such a flow is typically unusual near the sub-solar point in the equatorial magnetosheath. This hinders the determination of the actual frame of the x-point, which is needed for an outflow to be identified, despite the fact that the magnetic field, which is frame-independent, shows clear Hall signatures. It should be noted that, although we observe some typical signatures of reconnection, the evidence is far from conclusive. However, this current sheet is an interesting candidate to observe the properties of electron heating near high PVI intermittent structures, as discussed below.

The instrumental capabilities of the *MMS* spacecraft allow us to resolve the electron distribution functions within such thin structures in much more detail than in previous studies. In Figure 5, we examine the electron distribution functions and the spectra of the magnetic field for four different regions that have been highlighted in Figure 4. The first region corresponds to the plasma in the inflow region, outside the current sheet. The second and fourth regions correspond to the two edges of the current sheet, when the spacecraft cross the separatrices. The third region corresponds to the center of the current sheet, near the diffusion region, downstream of the x-line. We observe heating in the parallel direction in the two regions that lie at the edges of the current sheet, while at the center of the current sheet the electron distribution becomes isotropic again, though heated with respect to the plasma outside the current sheet. The heating pattern of the electrons, namely the strong parallel heating along the separatrices, appears to be consistent with kinetic simulations of magnetic reconnection (Shay et al. 2014). Additionally, at the first separatrix, shown in panel B of Figure 5, at low energies we observe an increased flux parallel to the magnetic field, whereas at higher energies there is an increased anti-parallel flux. On the other side of the current sheet, at the separatrix, this trend is reversed. This would be expected in such a case as the cold electrons flow toward the x-point, while energized electrons flow in the opposite direction.

The characteristics of the electron dynamics, namely, the increased electron flux and temperature in the direction parallel to the magnetic field at the edges of the current sheet, as well as the isotropic electron distributions in the center of the current sheet, are similar to observations of magnetic reconnection in the Earth's magnetopause reported by Lavraud et al. (2016).

It should be noted that the parallel heating of electrons at the edges of the current sheet is accompanied by large amplitude whistler waves. This is evidenced in magnetic field spectra, shown as insets for each panel of Figure 5. The vertical lines show the frequencies that correspond to $0.1\omega_c e$ and $1\omega_c e$ for each interval, where $\omega_c e$ is the electron cyclotron frequency. The peak between the two frequencies corresponds to strong waves in the whistler frequency regime. Along with this observed frequency range, the ellipticity (not shown here) is also consistent with whistler-like fluctuations.

6. Discussion

We have performed a statistical study of intermittent structures at kinetic scales in the Earth's magnetosheath, employing the unique high-resolution capabilities of instruments on the *MMS* spacecraft. We studied the electron heating within those structures, and examined one structure in detail, which in this case was a thin current sheet.

To survey the heating associated with structures, we have used the multi-spacecraft PVI technique. Coherent magnetic structures were identified within 3 minutes of burst data. We found statistical evidence suggesting that electron heating is enhanced in regions of high PVI. Specifically, the majority of the very strongly heated regions coincide with high PVI events.

High-resolution measurements of the electron distribution functions by the *MMS* spacecraft enable us, contrary to previous studies (Retinò et al. 2007; Chasapis et al. 2015), to directly examine the electron temperature at kinetic scales without any assumptions about the properties of the distribution functions.

Meanwhile, the multi-spacecraft nature of the mission, along with small spacecraft separation, allow us to focus exclusively on kinetic scale structures, which was not the case in single-spacecraft observations (Osman et al. 2011, 2014). Therefore, we are able to reliably establish a correlation between ion-scale structures and intermittent electron heating in turbulent plasma. The predominance of parallel electron heating at high PVI regions appears to be consistent with the assumption that magnetic reconnection dominates as a process in those cases (Servidio et al. 2011; Osman et al. 2014).

For the selected coherent structure, the observations suggested that this could be a region of ongoing magnetic reconnection. Although the data are not conclusive on this point, this current sheet is ideal to study electron heating in a high PVI intermittent structure. The data show that strong electron heating is located at the edges of this current sheet. Additionally, the electrons appear to be heated exclusively in the direction parallel to the magnetic field. High-frequency magnetic field measurements showed whistler-like wave emissions that coincide with the observed heating. In the center of the current sheet, the electron distributions become isotropic and moderately heated with respect to the electrons outside the current sheet.

The role of the whistler waves and possible wave-particle interactions warrants further investigation. Specifically, parallel electron heating along with whistlers could be an indication of modified two stream instability (e.g., McBride et al. 1972; Saito et al. 2015). However, the lack of perpendicularly heated protons (not shown here) makes such an instability less likely in our case. Even though whistler waves have been observed in sites of magnetic reconnection in the past (Deng & Matsumoto 2001; Fujimoto et al. 2011; Vaivads et al. 2011), more work will be needed to identify the exact relation between whistler waves and the observed parallel electron heating.

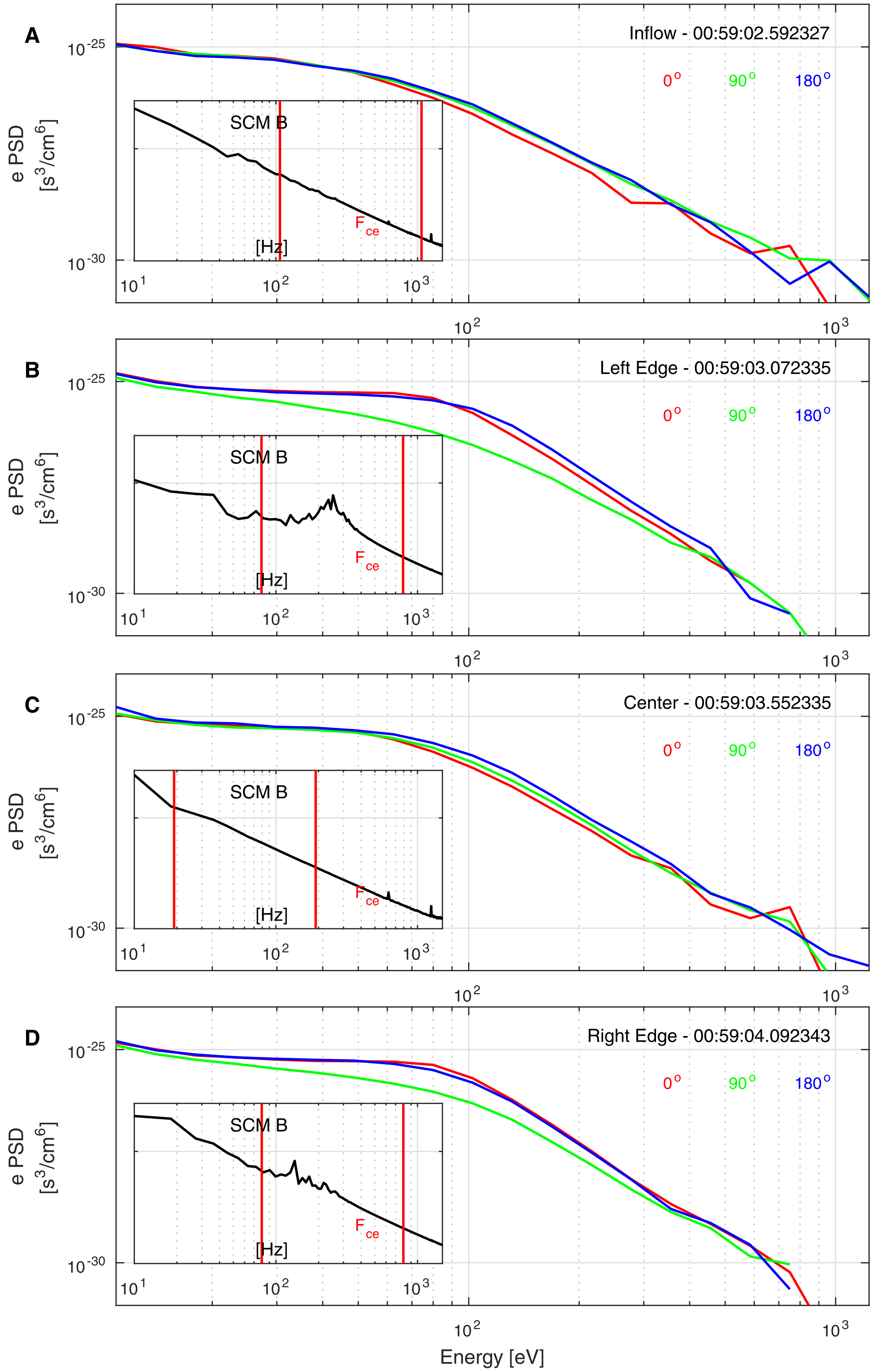

Figure 5. Electron distribution functions (e PSD) as a function of the energy, measured in the vicinity of the current sheet in the intervals highlighted in yellow in Figure 4. The inset plots (SCM B) show magnetic field spectra as a function of freqency in the same in the same intervals. Panels A, B, C, and D show, respectively, the inflow region, the right edge, the center, and the left edge of the current sheet as marked in Figure 4. The vertical red lines denote the frequencies that correspond to $0.1F_{ce}$ and $1F_{ce}$, where F_{ce} is the electron cyclotron frequency.

Regarding the specific mechanism behind the observed parallel heating of electrons, the field-aligned counter-streaming electrons, and the dynamics of the Hall currents, all of wave-particle interactions, field-aligned potentials and adiabatic trapping may play a role, as also purported for similar recent observations at the magnetopause by Lavraud et al. (2016). In that study, the population of field-aligned electrons is energized close to the x-line and travels downstream as it remains quasi-trapped.

A more detailed statistical study is needed in order to determine the underlying processes that lead to particle heating and dissipation at kinetic scales. Additionally, an in-depth analysis of individual current sheets will also provide valuable insight into the mechanisms at play. *MMS* data provides a valuable resource to examine these fundamental plasma physics issues.

This research partially supported by the *MMS* mission through NASA grant NNX14AC39G at the University of Delaware and in part by NSF-SHINE AGS-1460130. A. Chasapis is supported by the NASA grant. W. H. Matthaeus is a member of the *MMS* Theory and Modeling team. The French involvement (SCM instruments) on *MMS* is supported by CNES, CNRS-INSIS, and CNRS-INSU. We are grateful to the *MMS* instrument teams, especially SDC, FPI, and FIELDS, for cooperation and collaboration in preparing the data. The data used in this analysis are Level 2 FIELDS and FPI data products, in cooperation with the instrument teams and in accordance their guidelines. All *MMS* data are available at https://lasp.colorado.edu/mms/sdc/.

References

Baker, D. N., Riesberg, L., Pankratz, C. K., et al. 2016, SSRv, 199, 545
Bourouaine, S., & Chandran, B. D. G. 2013, ApJ, 774, 96
Burch, J. L., Moore, T. E., Torbert, R. B., & Giles, B. L. 2016, SSRv, 199, 5
Chasapis, A. 2015, PhD thesis, Univ. Paris IX
Chasapis, A., Retino, A., Sahraoui, F., et al. 2015, ApJL, 804, L1
Cirtain, J. W., Golub, L., Winebarger, A. R., et al. 2013, Natur, 493, 501
Deng, X. H., & Matsumoto, H. 2001, Natur, 410, 557
Dmitruk, P., & Matthaeus, W. H. 2006, PhPl, 13, 042307
Ergun, R. E., Tucker, S., Westfall, J., et al. 2016, SSRv, 199, 167
Fujimoto, M., Shinohara, I., & Kojima, H. 2011, SSRv, 160, 123
Gosling, J. T. 2007, ApJL, 671, L73
Greco, A., Chuychai, P., Matthaeus, W. H., Servidio, S., & Dmitruk, P. 2008, GeoRL, 35, 19111
Greco, A., Matthaeus, W. H., Servidio, S., Chuychai, P., & Dmitruk, P. 2009, ApJL, 691, L111
Haggerty, C. C., Shay, M. A., Drake, J. F., Phan, T. D., & McHugh, C. T. 2015, GeoRL, 42, 9657
Hasegawa, H., Wang, J., Dunlop, M. W., et al. 2010, GeoRL, 37, L16101
Hollweg, J. V., & Isenberg, P. A. 2002, JGRA, 107, 1147
Howes, G. G. 2015, RSPTA, 373, 20140145
Lavraud, B., Zhang, Y. C., Vernisse, Y., et al. 2016, GeoRL, 43, 3042
Le Contel, O., Leroy, P., Roux, A., et al. 2016, SSRv, 199, 257
Li, G. 2008, ApJL, 672, L65
Lindqvist, P. A., Olsson, G., Torbert, R. B., et al. 2016, SSRv, 199, 137
McBride, J. B., Ott, E., Boris, J. P., & Orens, J. H. 1972, PhFl, 15, 2367
Neugebauer, M. 2006, JGRA, 111, A04103
Osman, K. T., Matthaeus, W. H., Gosling, J. T., et al. 2014, PhRvL, 112, 215002
Osman, K. T., Matthaeus, W. H., Greco, A., & Servidio, S. 2011, ApJL, 727, L11
Parashar, T. N., & Matthaeus, W. H. 2016, ApJ, 832, 57
Parashar, T. N., Servidio, S., Shay, M. A., Breech, B., & Matthaeus, W. H. 2011, PhPl, 18, 092302
Paschmann, G., & Daly, P. W. 1998, Analysis Methods for Multi-spacecraft Data. ISSI Scientific Reports Series, SR-001 (Bern: ISSI)
Perrone, D., Alexandrova, O., Mangeney, A., et al. 2016, ApJ, 826, 196
Pollock, C., Moore, T., Jacques, A., et al. 2016, SSRv, 199, 331
Rappazzo, A. F., & Parker, E. N. 2013, ApJL, 773, L2
Ren, Y., Yamada, M., Gerhardt, S., et al. 2005, PhRvL, 95, 055003
Retinò, A., Sundkvist, D., Vaivads, A., et al. 2007, NatPh, 3, 236
Russell, C. T., Anderson, B. J., Baumjohann, W., et al. 2016, SSRv, 199, 189
Saito, S., Nariyuki, Y., & Umeda, T. 2015, PhPl, 22, 072105
Servidio, S., Greco, A., Matthaeus, W. H., Osman, K. T., & Dmitruk, P. 2011, JGRA, 116, A09102
Servidio, S., Valentini, F., Califano, F., & Veltri, P. 2012, PhRvL, 108, 045001
Shay, M. A., Haggerty, C. C., Phan, T. D., et al. 2014, PhPl, 21, 122902
Shibata, K., Nakamura, T., Matsumoto, T., et al. 2007, Sci, 318, 1591
Stevens, M. L. 2009, PhD thesis, Massachusetts Institute of Technology
Sundkvist, D., Retinò, A., Vaivads, A., & Bale, S. D. 2007, PhRvL, 99, 025004
Torbert, R. B., Russell, C. T., Magnes, W., et al. 2016, SSRv, 199, 105
Vaivads, A., Retinò, A., Khotyaintsev, Y. V., & André, M. 2011, AnGeo, 29, 1917
Wan, M., Matthaeus, W. H., Roytershteyn, V., et al. 2016, PhPl, 23, 042307
Xia, Q., Perez, J. C., Chandran, B. D. G., & Quataert, E. 2013, ApJ, 776, 90
Zhdankin, V., Uzdensky, D. A., Perez, J. C., & Boldyrev, S. 2013, ApJ, 771, 124